

Post-Synthetic Modifications of Framework Metal Ions in Isostructural Metal–Organic Frameworks: Core–Shell Heterostructures via Selective Transmetalations

Xiaokai Song,^{†,‡} Tae Kyung Kim,[†] Hye Hyun Kim,[†] Dongwook Kim,[†] Seok Jeong,[†] Hoi Ri Moon,[†] and Myoung Soo Lah^{*,†}

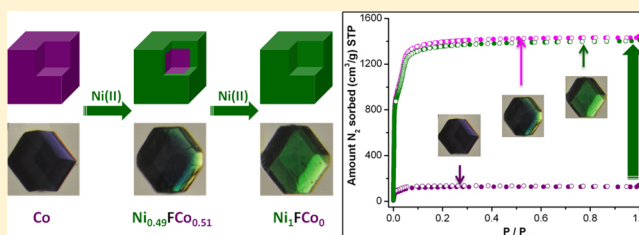
[†]Interdisciplinary School of Green Energy, Ulsan National Institute of Science & Technology, Ulsan, 689-805, Korea

[‡]Department of Chemistry and Applied Chemistry, Hanyang University, Ansan, Kyunggi-do, 426-791, Korea

Supporting Information

ABSTRACT: The transmetalation (the replacement of metal ions) of a family of highly porous isostructural metal–organic frameworks (MOFs), $M_6(\text{BTB})_4(\text{BP})_3$ (where $M = \text{Zn}(\text{II})$ (1), $\text{Co}(\text{II})$ (2), $\text{Cu}(\text{II})$ (3), and $\text{Ni}(\text{II})$ (4), BTB = 1,3,5-benzenetri benzoate, and BP = 4,4'-dipyridyl) with an *itb-d* net topology has been investigated. These compounds have different framework stabilities depending on the framework metal ions. The transmetalation and the reverse transmetalation reactions of the framework metal ions were observed between the MOFs, 1 and 2, having a similar thermodynamic stability. While the transmetalation from thermodynamically less stable 1 and 2 to more stable 3 and 4 were achieved by soaking single crystals of 1 and 2 in a solution of *N,N'*-dimethylformamide (DMF) containing $\text{Cu}(\text{II})$ and $\text{Ni}(\text{II})$ ions, respectively, no reverse transmetalation was observed. By simply controlling the soaking time, not only could homogeneously transmetalated crystalline framework structures be prepared via the thermodynamically controlled complete replacement of the framework metal ions but also selectively transmetalated core–shell heterostructures were formed via kinetically controlled replacement that was mainly restricted to the external shell region of the crystal. The fully transmetalated MOFs showed significantly improved framework stabilities compared with the parent MOFs. A marked improvement in the framework stability was observed, even in the selectively transmetalated $\text{Co}(\text{II})/\text{Cu}(\text{II})$ - and $\text{Co}(\text{II})/\text{Ni}(\text{II})$ -core–shell heterostructures. Although the frameworks are partially transmetalated, the framework stability of not only the external shell region but also of the internal core region was significantly affected.

KEYWORDS: porous metal–organic frameworks (MOFs), post-synthetic modification, framework metal ion exchange, transmetalation, core–shell heterostructure, framework stability



INTRODUCTION

The properties of metal–organic frameworks (MOFs) often need to be modified to meet the complicated requirements for diverse applications. The preparation of new isorecticular MOFs via similar synthetic procedures using modified building blocks containing new functional groups is often both complicated and frustrating. Post-synthetic modification (PSM) to the reactive sites of known MOFs is a frequently used strategy for obtaining modulated and functionalized MOFs.^{1–7} Covalent PSM using the reactive residues of organic linkers is well established,² and much work on dative PSMs of the metal centers and/or the organic linkers of MOFs has been reported.^{3,4} However, most work has been on modifications of the residues that are not directly involved in the network connectivity. The replacement of structural organic linkers or framework metal ions involved in the network connectivity is relatively rare. Recently, the preparation of an extended MOF via the replacement of a structural organic linker was reported.⁵ A previously unattainable pillared three-dimensional (3D) MOF was obtained by the replacement of a pillaring organic linker. The conversions of

MOFs to other isostructural MOFs via the replacement of a framework metal ion (i.e., transmetalation) has also been reported.⁶ Kim et al. reported on the complete transmetalation of a sodalite-like $\text{Cd}(\text{II})$ tricarboxylate MOF to the corresponding isostructural $\text{Pb}(\text{II})$ MOF while maintaining the structural integrity, and the reverse transmetalation of the $\text{Pb}(\text{II})$ MOF back to the $\text{Cd}(\text{II})$ MOF.^{6a}

On the other hand, as a strategy for preparing MOFs with multifunctional properties, the epitaxial growth of a shell MOF crystal on the external surface of a core MOF crystal to construct a multifunctional core–shell heterostructure has been employed.⁸ Another approach to obtaining a multifunctional MOF with a core–shell heterostructure is a PSM of the reactive residue of an organic linker that is not directly involved in the network connectivity. However, this modification is selectively constrained to either the external surface or the internal core of

Received: May 24, 2012

Revised: July 11, 2012

Published: July 16, 2012



the MOF. Gadzikwa et al. reported on the preparation of a core-shell heterostructure via selective modification of a MOF.⁹

A family of highly porous isostructural MOFs with a framework composition of $[M_6(\text{BTB})_4(\text{BP})_3]$ ($M = \text{Zn(II)}$, Co(II) , Cu(II) , and Ni(II) , $\text{BTB} = \text{benzene-1,3,5-tribenzoate}$, and $\text{BP} = 4,4'$ -bipyridyl) has been reported.¹⁰ The MOFs were prepared by linking BTB and BP as a three-connected node and a two-connected linker, respectively, with an $M(\text{II})$ paddle-wheel ($M_2(\text{COO})_4$) secondary building unit (SBU) as a six-connected node. In these MOFs, the axial sites of the paddle-wheel SBUs of the non-interpenetrated 3,4-connected network of a **pto** net topology are connected with BP molecules as linear ditopic linkers to form a 3,6-connected network of an **ith-d** net topology.¹¹ These MOFs, designated as **ITHD(M)**, according to the net topology, **ITHD(Zn)** (**1**), **ITHD(Co)** (**2**), **ITHD(Cu)** (**3**), and **ITHD(Ni)** (**4**), respectively, have different framework stabilities, depending on the framework metal ions, which makes them a good system for a systematic investigation into transmetalation of the framework metal ions. Recently, Zou et al. reported the framework metal ion exchange in the isostructural **ITHD** MOFs; however, the characterization on the properties of the exchanged MOF structures was limited.¹²

Here, we report on dative PSMs for isostructural MOFs of (a) homogeneously transmetalated framework structures with enhanced framework stabilities via thermodynamically controlled complete replacements of the framework metal ions, and (b) selectively transmetalated core-shell heterostructures via kinetically controlled replacements of the framework metal ions, mainly at the external shell region of the MOF crystals.

EXPERIMENTAL SECTION

General Procedures. All reagents used were purchased from commercial sources and used without further purification. Elemental analysis (C, H, and N) was performed at the Central Research Facilities of Ulsan National Institute of Science & Technology. Metal ions (Zn, Co, Ni, and Cu) were analyzed using a Varian 720-ES inductively coupled plasma atomic emission spectrometer (ICP-AES). FT-IR spectra were recorded using KBr pellets with a Nicolet iSIO FT-IR spectrophotometer ($4000\text{--}400\text{ cm}^{-1}$). Thermal gravimetric analysis (TGA) data were recorded using a TA Instruments Q-600 series thermal gravimetric analyzer under flowing nitrogen gas. Powder X-ray diffraction (PXRD) data were recorded using a Rigaku D/M 2200T automated diffractometer at room temperature, with a step size of 0.02° in 2θ angle. For the variable temperature PXRD (VT-PXRD) measurements, the samples were gradually heated from room temperature to the designated temperature in air with a holding time of at least 30 min at each temperature. Simulated PXRD patterns were calculated with the Material Studio software package¹³ employing the structural model from single crystal data.

Preparation of MOFs. A series of isostructural MOFs, $[M_6(\text{BTB})_4(\text{BP})_3] \cdot x\text{DMF} \cdot y\text{H}_2\text{O}$ (where x and y are the numbers of solvent N,N' -dimethylformamide (DMF) and water molecules in the solvent cavity, respectively), were prepared via solvothermal reactions that were slightly modified from the reported synthetic procedures.¹⁰

ITHD(Zn), 1. A solid mixture of $\text{Zn}(\text{NO}_3)_2 \cdot 6\text{H}_2\text{O}$ (38.2 mg, 0.128 mmol), H_3BTB (44.2 mg, 0.101 mmol), and BP (8.6 mg, 0.055 mmol) was dissolved in 5 mL of DMF in an 8 mL glass vial. The solution was then heated in an isotherm oven at 70°C for 1 d, resulting in colorless rhombic dodecahedral crystals being formed, which were collected by filtration and washed with fresh DMF. Yield = 55.6 mg, 46.0% based on BP. Elemental analysis for $\text{Zn}_6(\text{BTB})_4(\text{BP})_3(\text{DMF})_{46}(\text{H}_2\text{O})_{35} = \text{C}_{276}\text{H}_{476}\text{O}_{105}\text{N}_{52}\text{Zn}_6$ (fw = 6595.38 g/mol), calculated (%): C, 50.35; H, 7.37; N, 11.42. Found (%): C, 50.26; H, 7.27; N, 11.04. FT-IR (KBr , $4000\text{--}400\text{ cm}^{-1}$): 3445 (br, w), 3064 (w), 2929 (w), 1671 (vs), 1610 (s), 1557 (m), 1505 (w), 1494 (w), 1386 (s), 1255 (w), 1180

(w), 1095 (m), 1016 (w), 859 (m), 811 (w), 783 (m), 706 (w), 661 (w), 573 (w), 478 (w).

ITHD(Co), 2. A solid mixture of $\text{Co}(\text{NO}_3)_2 \cdot 6\text{H}_2\text{O}$ (39.9 mg, 0.137 mmol), H_3BTB (44.7 mg, 0.102 mmol), and BP (8.9 mg, 0.057 mmol) was dissolved in 5 mL of DMF. The solution was divided into five portions in a Pyrex tube and heated in an isotherm oven at 100°C for 4 d, resulting in dark-purple rhombic dodecahedral crystals being formed, which were collected by filtration and washed with fresh DMF. Yield = 103 mg, 83.7% based on BP. Elemental analysis for $\text{Co}_6(\text{BTB})_4(\text{BP})_3(\text{DMF})_{45}(\text{H}_2\text{O})_{35} = \text{C}_{273}\text{H}_{469}\text{O}_{104}\text{N}_{51}\text{Co}_6$ (fw = 6483.61 g/mol), calculated (%): C, 50.57; H, 7.29; N, 11.02. Found (%): C, 50.19; H, 6.81; N, 11.50. FT-IR (KBr , $4000\text{--}400\text{ cm}^{-1}$): 3420 (br, w), 3065 (w), 2929 (w), 1669 (vs), 1607 (s), 1591 (s), 1539 (m), 1388 (vs), 1255 (w), 1220 (w), 1180 (w), 1120 (w), 1067 (m), 1016 (w), 859 (m), 811 (w), 783 (m), 706 (w), 667 (w), 574 (w), 477 (w).

ITHD(Cu), 3. A solid mixture of $\text{Cu}(\text{OAc})_2 \cdot \text{H}_2\text{O}$ (8.26 mg, 0.0414 mmol), and H_3BTB (8.69 mg, 0.0198 mmol) was dissolved in a 3.0 mL DMF/ethanol/ H_2O (2/2/1 ratio) mixed solvent in a 8 mL glass vial. A 0.5 mL of 1 M HNO_3 was added to the solution, and then BP (1.76 mg, 0.0113 mmol) was added. The reaction solution was heated in an isotherm oven at 70°C for 1 d, resulting in cyan rhombic dodecahedral crystals being formed, which were collected by filtration and washed with fresh DMF and ethanol. Yield = 22.6 mg, 90.9% based on BP. Elemental analysis for $\text{Cu}_6(\text{BTB})_4(\text{BP})_3(\text{DMF})_{42}(\text{H}_2\text{O})_{52} = \text{C}_{264}\text{H}_{482}\text{O}_{118}\text{N}_{48}\text{Cu}_6$ (fw = 6598.26 g/mol), calculated (%): C, 48.06; H, 7.36; N, 10.19. Found (%): C, 48.00; H, 7.20; N, 10.19. FT-IR (KBr , $4000\text{--}400\text{ cm}^{-1}$): 3461 (br, w), 3066 (w), 2929 (w), 1674 (vs), 1608 (s), 1554 (m), 1506 (w), 1404 (s), 1388 (s), 1255 (w), 1220 (w), 1182 (w), 1094 (m), 1016 (w), 858 (m), 812 (w), 783 (m), 708 (w), 668 (w), 573 (w), 516 (w), 485 (w).

ITHD(Ni), 4. A solid mixture of $\text{Ni}(\text{NO}_3)_2 \cdot 6\text{H}_2\text{O}$ (39.3 mg, 0.135 mmol), H_3BTB (44.7 mg, 0.102 mmol), and BP (8.9 mg, 0.057 mmol) was dissolved in 5 mL of DMF in an 8-mL glass vial. The solution was heated in an isotherm oven at 100°C for 4 d, resulting in green rhombic dodecahedral crystals being formed, which were collected by filtration and washed with fresh DMF. The product was obtained as a pure crystalline form using this modified synthetic procedure, unlike the reported procedure.^{10b} Yield = 113 mg, 89.0% based on BP. Elemental analysis for $\text{Ni}_6(\text{BTB})_4(\text{BP})_3(\text{DMF})_{50}(\text{H}_2\text{O})_{26} = \text{C}_{288}\text{H}_{486}\text{O}_{100}\text{N}_{56}\text{Ni}_6$ (fw = 6685.48 g/mol), calculated (%): C, 51.74; H, 7.33; N, 11.73. Found (%): C, 52.03; H, 6.85; N, 12.05. FT-IR (KBr , $4000\text{--}400\text{ cm}^{-1}$): 3420 (br, w), 3067 (w), 2930 (w), 1668 (vs), 1607 (s), 1589 (s), 1539 (m), 1388 (vs), 1255 (w), 1220 (w), 1180 (w), 1096 (w), 1068 (m), 1016 (w), 860 (m), 812 (w), 783 (m), 708 (w), 668 (w), 574 (w), 478 (w).

Transmetalation of the Framework Metal Ions. Before the transmetalation of the MOFs, the as-synthesized single crystals of **1**, **2**, **3**, and **4** were soaked in DMF for 2 d to remove any remaining reactants and side products present in the solvent cavities, respectively. During the soaking process, the solvent was refreshed twice. After soaking the MOF crystals in the corresponding metal ion DMF solution, the solvent was decanted, and then the transmetalated MOF crystals were harvested by filtration, washed thoroughly with DMF, and then kept in fresh DMF for 1 d to remove the excess metal salt from the solvent pores of the framework. $\text{N}_x\text{FM}_{1-x}$ is used as a general notation for a transmetalated MOF, where, **N** represents the framework structure with the replaced framework metal ion, **M** represents the framework structure with the initial framework metal ion, the subscript x in N_x represents the mole fraction of the replaced metal ion after the transmetalation, and the subscript $1-x$ in M_{1-x} represents the mole fraction of the remaining initial metal ion in the framework structure.

1F₂₀ and 2F₁₀. The purple crystals of **2** and the colorless crystals of **1** refreshed in DMF solvent were soaked in 0.1 M $\text{Zn}(\text{NO}_3)_2 \cdot 6\text{H}_2\text{O}$ and 0.1 M $\text{Co}(\text{NO}_3)_2 \cdot 6\text{H}_2\text{O}$ DMF solutions, respectively, at ambient temperature for 2 d.

3F₁₀, 3F₂₀, and 3F₄₀. The colorless crystals of **1**, the purple crystals of **2**, and the green crystals of **4** refreshed in DMF solvent were

soaked in 0.1 M $\text{Cu}(\text{NO}_3)_2 \cdot 2.5\text{H}_2\text{O}$ DMF solution, respectively, at an ambient temperature for 2 d, 1d, and 15 d.

4₁F₁₀ and 4₁F₂₀. The colorless crystals of **1** and the purple crystals of **2** refreshed in DMF solvent were soaked in 0.1 M $\text{Ni}(\text{NO}_3)_2 \cdot 6\text{H}_2\text{O}$ DMF, respectively, at 100 °C for 2 and 1 d.

Kinetic Studies of the Transmetalation. In the kinetic studies of the transmetalation, approximately equal amounts of the as-synthesized ITHD crystals were soaked in 0.1 M metal nitrate DMF solutions. After decanting the metal solutions, the soaked samples were washed thoroughly using DMF, kept in fresh DMF for 1 d to remove the excess metal salts from the solvent pores of the frameworks, soaked in dichloromethane (MC) for 2 d, and then dried under vacuum at room temperature overnight before being subjected to ICP-AES analysis to determine the metal contents.

Procedure for Epitaxially Grown Core–Shell MOF. Before the preparation of core–shell MOF crystals, the as-synthesized single crystals of **2**, **3**, and **4** were soaked in fresh DMF solvent for 2 d. During the soaking, the solvent was refreshed twice. $\text{M}@N$ is used as a general notation for the epitaxially prepared core–shell MOFs, where, N is the core crystal and M is the shell crystal.

1@2, 1@3, and 1@4. The purple seed crystals of **2**, the cyan seed crystals of **3**, and the green seed crystals of **4** were soaked in 5 mL of DMF solution of $\text{Zn}(\text{NO}_3)_2 \cdot 6\text{H}_2\text{O}$ (38.2 mg, 0.128 mmol), H_3BTB (44.2 mg, 0.10 mmol), and BP (8.6 mg, 0.055 mmol), at an ambient temperature for 3 d. **1@2**, **1@3**, and **1@4** core–shell crystals with a small fraction of **1** single crystals were harvested by filtration and washed with fresh DMF.

Activation of MOFs Using a Conventional Vacuum Drying (CVD) Process. The following specific procedure was used for the activation of all the MOFs via a CVD process. The as-synthesized and the transmetalated ITHD MOF crystals were soaked in MC for 2 d: the solvent MC was refreshed three times during the soaking process. The resulting MC-soaked samples were transferred as a suspension in a BET-sample-cell, and the solvent was decanted. The wet sample was then evacuated at room temperature for 1 d.

Activation of MOFs Using a Supercritical Carbon Dioxide Drying (SCD) Process.¹⁴ The as-synthesized and the transmetalated ITHD MOF crystals were soaked in DMF for 2 d: the solvent DMF was refreshed three times during the soaking. In the cases of **1** and **2**, freshly distilled anhydrous DMF solvent was used. The sample was evacuated using supercritical CO_2 in a Tousimis Samdri PVT-3D critical point dryer. The sample in fresh DMF solvent was placed in the chamber, and the DMF was fully exchanged with liquid CO_2 . The CO_2 filling was kept for 2 h and then followed by a purge vent for 10 min, which was repeated five times before heating. The chamber containing the sample and liquid CO_2 was heated to around 40 °C and kept under the supercritical condition (typically 1300 psi) for 1 h. The CO_2 was slowly vented overnight from the chamber at 40 °C.

N_2 Sorption Measurements. All N_2 sorption isotherms were measured using a BELSORP-max (BEL Japan, Inc.) employing a standard volumetric technique up to saturated pressure at 77 K. The adsorption data in the pressure range lower than $\sim 0.1 P/P_0$ were fitted to the Brunauer–Emmett–Teller (BET) equation to determine the BET specific surface areas. The entire set of adsorption data was used to obtain the Langmuir specific surface area.

RESULT AND DISCUSSION

In this study, we prepared a series of the isostructural ITHD MOFs via solvothermal reactions of H_3BTB and BP with $\text{M}(\text{II})$ salts in DMF. The bulk identities and the phase purities of the MOFs were confirmed using a combination of elemental analysis and a comparison of the simulated PXRD pattern from the single crystal structure of **1** with the observed PXRD patterns of the bulk crystals of all the ITHD MOFs (Figure 1).

The TGA data of the isostructural porous MOFs in a flowing N_2 environment indicated various thermal stabilities, depending on the framework metal ion present, even though the MOFs have exactly the same framework structure, except for the metal

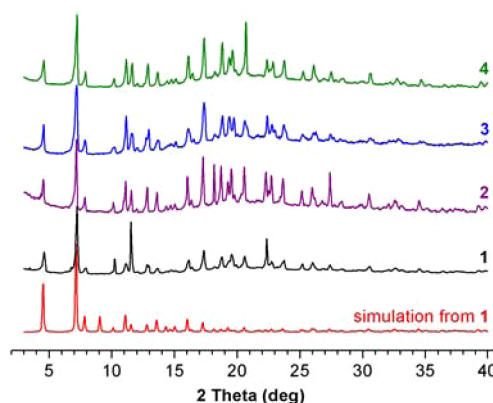


Figure 1. PXRD patterns of the as-synthesized MOFs: **1** (black), **2** (purple), **3** (blue), and **4** (green). The simulated PXRD pattern of **1** (red) is from the single crystal structure of **1**.

ion present. The TGA data of **1** and **2** were very similar (Figure 2, Supporting Information, Figures S1 and S2). A rapid $\sim 60\%$

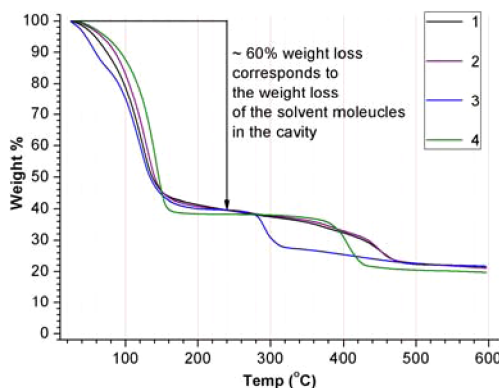


Figure 2. TGA data of the as-synthesized MOFs: **1** (black), **2** (purple), **3** (blue), and **4** (green).

weight loss up to ~ 180 °C occurred, followed by a subsequent gradual $\sim 5\%$ weight loss up to ~ 330 °C. Then, an additional gradual two-step weight loss occurred up to ~ 470 °C. The thermal behavior of **3** was also similar to that of **1** and **2** up to 170 °C (Figure 2 and Supporting Information, Figure S3). After the first weight loss up to ~ 170 °C for the solvent molecules in the cavity, no significant weight loss occurred up to ~ 270 °C for **3**, and then a gradual additional two-step weight loss occurred up to ~ 470 °C. The TGA data of **4** indicated that the framework structure was stable up to ~ 350 °C after the first $\sim 61\%$ weight loss (Figure 2 and Supporting Information, Figure S4).

The variable temperature PXRD (VT-PXRD) patterns of the as-synthesized MOFs in air, **1–4**, also support the different thermal stabilities of the framework structures of the ITHD MOFs (Supporting Information, Figures S5–S8). Even though the TGA data of **1–3** indicate that the framework weight loss starts around 170–180 °C, the diffraction peaks of **1–3** at ~ 50 °C had already significantly broadened, and **1–3** lose their crystallinities completely at 200 °C. Although the TGA data of the as-synthesized **3** in an N_2 environment showed the possibility of the framework being stable up to ~ 270 °C, the VT-PXRD patterns of **3** in air indicated a limited thermal stability of the framework structure.¹⁵ As shown in Figure S8, the thermal stability of the framework structure of as-

synthesized **4** up to ~ 350 °C in VT-PXRD even in air was remarkable, especially considering an $\sim 80\%$ solvent cavity of the ITHD network structure.

The porosities and the framework stabilities of the isostructural MOFs activated via two different processes, CVD and SCD, could also be assessed from the N_2 sorption measurements (Figure 3). While **1** activated via a CVD process

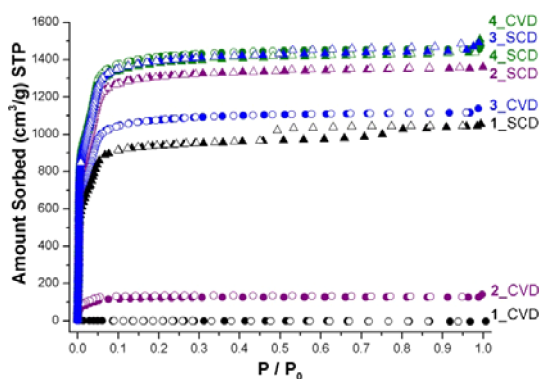


Figure 3. N_2 sorption isotherms of **1** (black), **2** (purple), **3** (blue), and **4** (green) at 77 K. The spherical symbols denote the isotherms of the samples activated via the CVD process, and the triangular symbols denote the isotherms of the samples activated via the SCD process (the solid and open shapes represent adsorption and desorption isotherms, respectively).

lost its crystallinity and did not show any N_2 adsorption at 77 K, as has been reported,¹⁰ **1** activated via a SCD process kept its crystallinity and showed a type I sorption isotherm with a BET specific surface area of $3710 \text{ m}^2 \text{ g}^{-1}$ and an N_2 adsorption of $1044 \text{ cm}^3 \text{ g}^{-1}$. The BET specific surface area was slightly smaller than the reported values for the same MOFs, FJI-1(Zn) and DUT-23(Zn) (Table 1). Considering the extremely large solvent cavities of the ITHD framework, **2** activated via the CVD process again showed a relatively small BET specific surface area ($480 \text{ m}^2 \text{ g}^{-1}$), with an N_2 adsorption of $127 \text{ cm}^3 \text{ g}^{-1}$. However, **2** activated via the SCD process had a BET specific surface area of $5200 \text{ m}^2 \text{ g}^{-1}$, with an N_2 adsorption of $1361 \text{ cm}^3 \text{ g}^{-1}$, which is larger than the reported values for DUT-23(Co) and is even larger than the geometrically calculated specific surface area of **1**, $5058 \text{ m}^2 \text{ g}^{-1}$, reported by Kaskel et al.^{10b} The BET specific surface area of **3** activated via the CVD process was $4260 \text{ m}^2 \text{ g}^{-1}$, with an N_2 adsorption of $1116 \text{ cm}^3 \text{ g}^{-1}$, which was significantly larger than those of **1** and **2**. The BET specific surface area of **3** activated via the SCD process, was $5480 \text{ m}^2 \text{ g}^{-1}$. The BET specific surface areas of **4** activated via CVD and SCD processes are 5590 and $5470 \text{ m}^2 \text{ g}^{-1}$, respectively. The similar BET specific areas of **4**, regardless the activation processes used, strongly support the relatively high framework stability of the Ni-based ITHD network structure.

The different framework stabilities, together with the high porosity of this family of the isostructural MOFs, prompted us to explore the possibility of the framework metal ion exchange. The transmetalation and the reverse transmetalation of the framework metal ions were observed for **1** and **2**. Transmetalated **1**₁F₂₀ crystals (**1** obtained from **2** via complete replacement of the framework metal ion) and transmetalated **2**₁F₁₀ crystals (**2** obtained from **1** via complete replacement of the framework metal ion) could be obtained within a period of 2 d. Optical microscopic photographs of a single crystal of **1** in

Table 1. BET Specific Surface Areas and the Total Pore Volumes of the As-Synthesized and the Transmetalated ITHD MOFs

ITHD MOFs	$S_{\text{ABET}}^{\text{CVD}} \text{ m}^2 \text{ g}^{-1}$ ^a	$S_{\text{ABET}}^{\text{SCD}} \text{ m}^2 \text{ g}^{-1}$ ^a	$(V_p^{\text{CVD}})^{\text{a}}$ $\text{cm}^3 \text{ g}^{-1}$	$(V_p^{\text{SCD}})^{\text{a}}$ $\text{cm}^3 \text{ g}^{-1}$	ref.
FJI-1(Zn)	ND ^b	4043	ND	1.43	10a
DUT-23(Zn)	ND	4340	ND	1.85	10b
DUT-23(Co)	ND	4850	ND	2.03	10b
DUT-23(Cu)	ND	4730	ND	2.01	10b
1 (Zn)	0	3710	0	1.62	this work
2 (Co)	480	5200	0.20	2.10	this work
3 (Cu)	4260	5480	1.76	2.24	this work
4 (Ni)	5590	5470	2.25	2.25	this work
3 ₁ F ₁ ₀	3130	ND	1.28	ND	this work
3 ₁ F ₂ ₀	3200	ND	1.30	ND	this work
3 _{0.83} F ₄ _{0.17}	3740	ND	1.52	ND	this work
4 ₁ F ₁ ₀	5310	ND	2.13	ND	this work
4 ₁ F ₂ ₀	5330	ND	2.18	ND	this work

^aThe BET specific surface areas (S_{ABET}) of the ITHD MOFs activated via the CVD and the SCD process obtained from the N_2 adsorption isotherms. The total pore volume (V_p) was estimated from the N_2 adsorption amounts assuming that the density of N_2 in the pores around the saturation pressure at 77 K was the same as that of liquid N_2 at 77 K. ^bNo data were reported or measured.

0.1 M Co(II) DMF solution and a single crystal of **2** in 0.1 M Zn(II) DMF solution show that the color changes occurred in the crystals while keeping the crystal integrity during the framework metal ion replacement (Figure 4). In the case of **2**, the gradual color change in color, from purple to colorless, was observed from the surface of the crystal to the center of the crystal during the transmetalation of Co(II) with Zn(II) in the framework (Figure 4b). This indicates that the metal ion exchange proceeded selectively from the external surface to the internal core of the framework. The transmetalated **2**₁F₁₀ and **1**₁F₂₀ crystals retained their parent framework structures, as confirmed by the PXRD patterns (Supporting Information, Figure S9). The transmetalation and the reverse transmetalation of the framework metal ions were monitored using the ICP-AES analysis of the mole fractions of the framework metal ions, Zn(II) and Co(II) (Figure 5).

Optical microscopic photographs of single crystals of **1**, **2**, and **4** in a 0.1 M Cu(II) DMF solution are shown in Figure 6. As in the case of the **1**₁F₂₀ crystal, when the transmetalation of the framework metal ion proceeded from Co(II) to Cu(II), the cyan colored external layer of the crystal resulted from the replacement of Co(II) with Cu(II) in the framework, which became thicker with gradual disappearance of the blue color at the center of the crystal (Figure 6b) (blue resulted from a mixture of the cyan and the purple colors). The structural integrity of the frameworks after transmetalation to **3**₁F₁₀, **3**₁F₂₀, and **3**₁F₄₀ was once again confirmed from PXRD patterns (Supporting Information, Figure S10). The ICP-AES

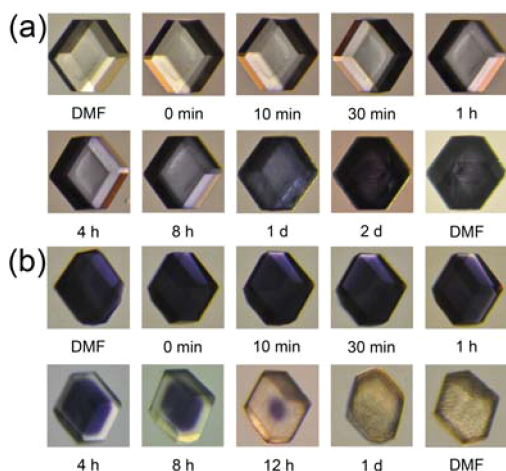


Figure 4. Optical microscopic photographs of (a) a single crystal of **1** ($0.45 \times 0.45 \times 0.34$ mm in size) in 0.1 M $\text{Co}(\text{NO}_3)_2 \cdot 6\text{H}_2\text{O}$ DMF solution, and (b) a single crystal of **2** ($0.26 \times 0.26 \times 0.20$ mm in size) in 0.1 M $\text{Zn}(\text{NO}_3)_2 \cdot 6\text{H}_2\text{O}$ DMF solution at an ambient temperature. The first and the last photographs in (a) and (b) show the single crystals in a fresh DMF solvent before and after the transmetalation, respectively. The photographs between the first and the last photographs show single crystals in the metal salt DMF solutions for different periods.

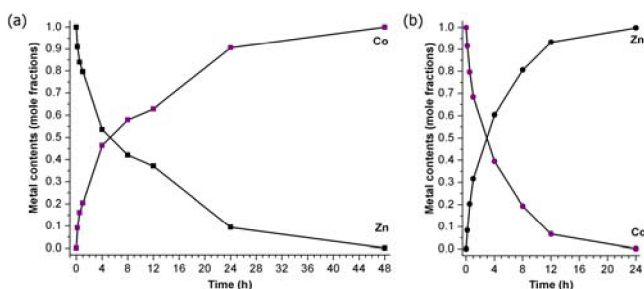


Figure 5. Framework metal ion contents in mole fractions during transmetalation of the ITHD framework structures: (a) From **1** to **2**, and (b) from **2** to **1**.

analysis showed that the framework metal ion exchanges in 3_1F_1 and 3_1F_2 were complete within a period of 1 d (Supporting Information, Figure S11). However, the transmetalation of the framework metal ion in 3_1F_4 occurred much more slowly. The ICP-AES shows that the sample soaked for a week had an 83% transmetalation of the framework metal ion, and full transmetalation required about two weeks. Thermally stable **4** in solid state is kinetically inert in DMF solution. Unlike the cases of **1** and **2**, while the transmetalations from **1**, **2**, and **4** to **3** are possible, the reverse transmetalations do not occur, which strongly indicates that **3**, based on $\text{Cu}_2(\text{COO})_4$ SBU, is thermodynamically the most stable MOF among this family of MOFs.

During the transmetalations of the framework metal ions from Zn(II) to Cu(II) and from Co(II) to Cu(II), not only was the structural integrity of the frameworks kept but also the framework stabilities were enhanced (Figure 7 and Supporting Information, Figure S12; Table S1). While **1** activated via the CVD process does not show any N_2 adsorption at 77 K, 3_1F_1 kept its crystallinity and showed a type I sorption isotherm with a BET specific surface area of $3130 \text{ m}^2 \text{ g}^{-1}$ and an N_2 adsorption of $824 \text{ cm}^3 \text{ g}^{-1}$ (Figure 7 and Supporting Information, Figure S10; Table S1). The BET specific surface

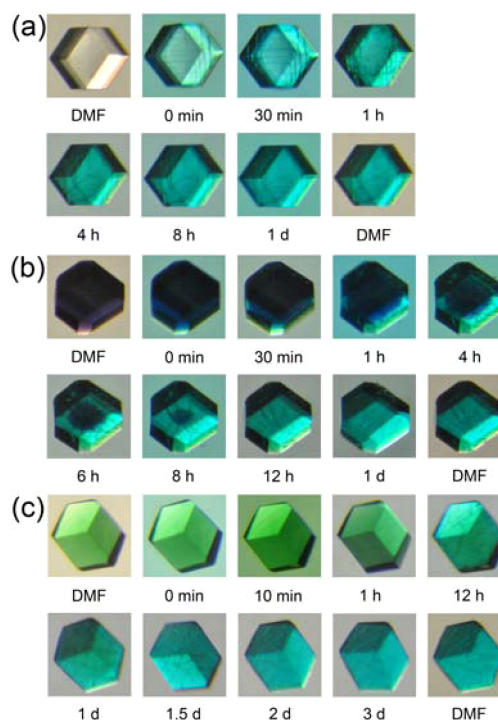


Figure 6. Optical microscopic photographs of (a) a single crystal of **1** ($0.45 \times 0.45 \times 0.34$ mm in size), (b) a single crystal of **2** ($0.26 \times 0.26 \times 0.20$ mm in size), and (c) a single crystal of **4** ($0.12 \times 0.12 \times 0.12$ mm in size) in a 0.1 M $\text{Cu}(\text{NO}_3)_2 \cdot 2.5\text{H}_2\text{O}$ DMF solution at ambient temperature, respectively. The first and the last photographs in (a–c) show single crystals in fresh DMF solvent before and after the transmetalation. The photographs between the first and the last photographs show single crystals in the metal salt DMF solution for different periods.

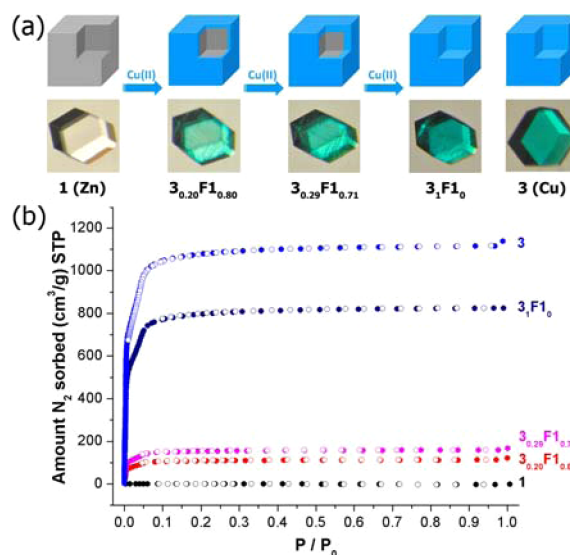


Figure 7. (a) Optical photographs of an as-synthesized crystal of **1**, its transmetalated $3_{0.20}\text{F}_1$, $3_{0.29}\text{F}_1$, and 3_1F_1 crystals, and an as-synthesized crystal of **3** with the corresponding schematic drawings of the core–shell heterostructures. (b) The N_2 sorption isotherms of **1** (black), $3_{0.20}\text{F}_1$ (red), $3_{0.29}\text{F}_1$ (magenta), 3_1F_1 (navy), and **3** (blue) activated via the CVD process at 77 K (solid and open shapes denote adsorption and desorption, respectively).

area and N_2 adsorption of 3_1F_1 were $\sim 73\%$ of those of as-synthesized **3**. Not only could the extent of the transmetalation

be kinetically modulated by controlling the soaking time but also the location of the transmetalation could be selectively restrained mainly at the external surface or shell region of the crystalline sample to form a core–shell heterostructure. Selectively transmetalated $3_{0.12}\text{F1}_{0.88}$, $3_{0.20}\text{F1}_{0.80}$, and $3_{0.29}\text{F1}_{0.71}$ were also obtained simply by soaking the single crystals of **1** in a Cu(II) DMF solution for 10 min, 30 min, and 1 h, respectively (Supporting Information, Figure S11). Notably, the optical microscopic photograph of a face-cut $3_{0.12}\text{F1}_{0.88}$ crystal clearly showed the cyan color of the transmetalated framework metal ion was constrained only on the external surface of the crystal while keeping the internal core colorless (Figure 8). This strongly indicates that $3_{0.12}\text{F1}_{0.88}$

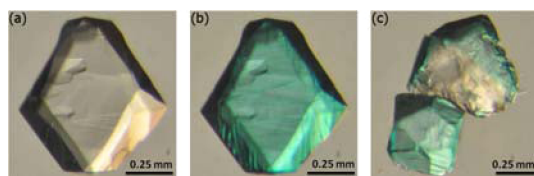


Figure 8. Optical microscopic photograph of a face-cut $3_{0.12}\text{F1}_{0.88}$ crystal. The photographs show a single crystal of **1** (a) before and (b) after soaking in a 0.1 M $\text{Cu}(\text{NO}_3)_2 \cdot 2.5\text{H}_2\text{O}$ DMF solution for 10 min at ambient temperature, respectively. (c) The bottom left-hand fragment of the face-cut crystal after soaking shows the cyan colored external surface, and the top right-hand fragment shows the colorless internal region of the crystal with a cyan-colored external shell.

is a core–shell heterostructure. The core–shell heterostructures, $3_{0.20}\text{F1}_{0.80}$ and $3_{0.29}\text{F1}_{0.71}$, had BET specific surface areas of 420 and 600 $\text{m}^2 \text{g}^{-1}$, respectively, and these recoveries of the BET specific surface areas of 13% and 19% compared with the BET specific surface area of the fully converted 3_1F1_0 are mainly attributed from the stable “shell” structure of the core–shell heterostructures.

3_1F2_0 activated via the CVD process also showed a similar marked enhancement in porosity, with a BET specific surface area of 3200 $\text{m}^2 \text{g}^{-1}$ and an N_2 adsorption of 845 $\text{cm}^3 \text{g}^{-1}$, compared with the porosity of **2** (Supporting Information, Figure S12 and Table S1). The BET specific surface area and the N_2 adsorption of 3_1F2_0 were $\sim 75\%$ of those of **3**. More interestingly, the BET specific surface areas of the selectively transmetalated core–shell heterostructures, $3_{0.32}\text{F2}_{0.68}$ and $3_{0.36}\text{F2}_{0.64}$ obtained by soaking **2** in a Cu(II) DMF solution for 10 and 30 min, respectively, was similar to, or even larger than, the BET specific surface area of the fully transmetalated 3_1F2_0 . Unlike the similar core–shell heterostructures $3_{0.32}\text{F1}_{0.68}$ and $3_{0.36}\text{F1}_{0.64}$, although $3_{0.32}\text{F2}_{0.68}$ and $3_{0.36}\text{F2}_{0.64}$ were partially transmetalated, the full recovery of the framework stability was observed, and the partial and selective transmetalation in the “shell” region of the structure influenced the stability of the “shell” region and also “core” region of the framework.

The BET specific surface area and the N_2 adsorption of $3_{0.83}\text{F4}_{0.17}$ were smaller than those of **4** but also **3** (Supporting Information, Figure S13). The framework stability of the transmetalated framework, $3_{0.83}\text{F4}_{0.17}$, was lower than the corresponding as-synthesized MOFs, **3** and **4**, although the transmetalation was from **4**, the MOF with the highest framework stability in the solid state, to **3**, the MOF with the thermodynamically most stable framework in solution.

The complete transmetalation of the framework metal ions, Zn(II) and Co(II) ions in **1** and **2** to Ni(II) ions, was achieved

when the crystals were soaked in a Ni(II) DMF solution at 100 °C. Optical microscopic photographs of single crystals of **1** and **2** after soaking in a 0.1 M Ni(II) DMF solution at 100 °C are also shown in Figure 9. The gradual change in color from

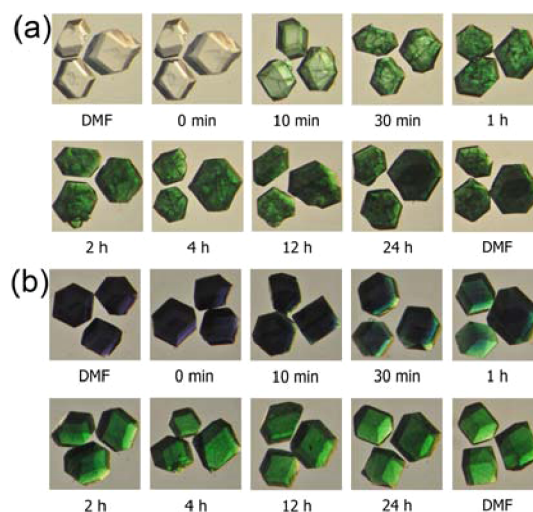


Figure 9. Optical microscopic photographs of three single crystals of (a) **1** and (b) **2** in a 0.1 M $\text{Ni}(\text{NO}_3)_2 \cdot 6\text{H}_2\text{O}$ solution at 100 °C, respectively. The first and the last photographs in (a) and (b) show single crystals in fresh DMF solvent before and after the transmetalation. The photographs between the first and the last photographs show single crystals in the metal salt DMF solution for different periods.

purple to green during the transmetalation of the framework structure from **2** to **4** was observed from the external surface of the crystals to the center of the crystals. The ICP-AES analysis showed that the transmetalations of the framework metal ions for 4_1F1_0 and 4_1F2_0 was complete within a period of 2 d (Supporting Information, Figure S14). The transmetalated 4_1F1_0 and 4_1F2_0 retained their parent framework structures, confirmed from PXRD patterns (Supporting Information, Figure S15).

The N_2 adsorption and the BET specific surface area of 4_1F1_0 activated via the CVD process are 1390 $\text{cm}^3 \text{g}^{-1}$ and 5310 $\text{m}^2 \text{g}^{-1}$, respectively, which are similar to those of as-synthesized **4** activated via the CVD process (Supporting Information, Figure S16 and Table 2). Kinetically modulated partial transmetalations via controlling the soaking time at 100 °C again led to selectively transmetalated core–shell

Table 2. BET Specific Surface Area, the Langmuir Surface Area, and the Total Pore Volume of the Transmetalated 4_xF1_{1-x} and 4_xF2_{1-x} Which Were Activated via the CVD Process

MOFs	$\text{SA}_{\text{BET}} \text{m}^2 \text{g}^{-1}$	$A_{\text{Lang}} \text{m}^2 \text{g}^{-1}$	$V_p \text{cm}^3 \text{g}^{-1}$
1 (Zn)	0	0	0
$4_{0.22}\text{F1}_{0.78}$	1230	1320	0.47
$4_{0.30}\text{F1}_{0.70}$	2320	2420	0.86
4_1F1_0	5310	6020	2.13
2 (Co)	480	560	0.20
$4_{0.34}\text{F2}_{0.64}$	5330	6070	2.15
$4_{0.49}\text{F2}_{0.51}$	5500	6260	2.22
4_1F2_0	5330	6110	2.18
4 (Ni)	5590	6370	2.25

heterostructures, $4_{0.22}\text{F}1_{0.78}$ (10 min soaking) and $4_{0.30}\text{F}1_{0.70}$ (30 min soaking) (Supporting Information, Figure S14). The BET specific surface areas of $4_{0.22}\text{F}1_{0.78}$ and $4_{0.30}\text{F}1_{0.70}$ are $1230\text{ m}^2\text{ g}^{-1}$ and $2320\text{ m}^2\text{ g}^{-1}$, respectively, and these values were $\sim 23\%$ and $\sim 44\%$ of the BET specific surface area of $4_1\text{F}1_0$. As in the cases of the core–shell heterostructures of $3_{0.20}\text{F}1_{0.80}$ and $3_{0.29}\text{F}1_{0.71}$, the framework stabilization of the core–shell heterostructures, $4_{0.22}\text{F}1_{0.78}$ and $4_{0.30}\text{F}1_{0.70}$, was related to the extent of transmetalation, and the stabilization was limited to the transmetalated “shell” region of the frameworks.

The N_2 adsorption and the BET specific surface area of $4_1\text{F}2_0$ activated via the CVD process are $1362\text{ cm}^3\text{ g}^{-1}$ and $5240\text{ m}^2\text{ g}^{-1}$, respectively, which again are similar to those of as-synthesized **4** activated via the CVD process (Figure 10 and

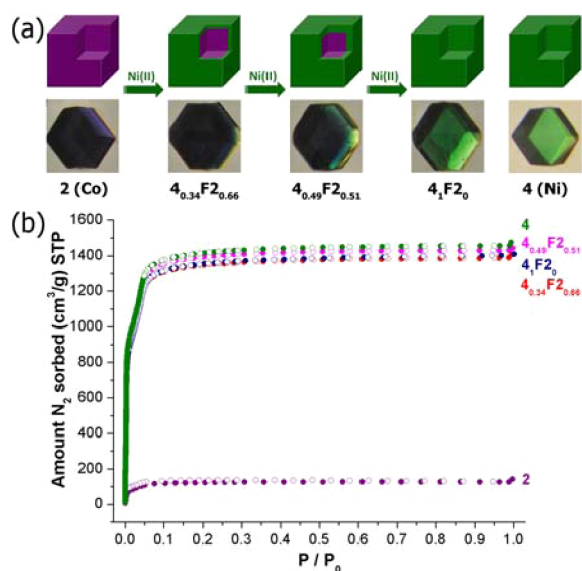


Figure 10. (a) Optical photographs of an as-synthesized **2** crystal, its transmetalated $4_{0.34}\text{F}2_{0.66}$, $4_{0.49}\text{F}2_{0.51}$, and $4_1\text{F}2_0$ crystals, and an as-synthesized **4** crystals with the corresponding schematic drawings of the core–shell heterostructures. (b) The N_2 sorption isotherms of **2** (purple), $4_{0.34}\text{F}2_{0.66}$ (red), $4_{0.49}\text{F}2_{0.51}$ (magenta), $4_1\text{F}2_0$ (navy), and **4** (green) activated via the CVD process at 77 K (solid and open shapes represent adsorption and desorption, respectively).

Table 2). Remarkably, the BET specific surface areas of the selectively transmetalated core–shell heterostructures, $4_{0.34}\text{F}2_{0.66}$ (10 min soaking at $100\text{ }^\circ\text{C}$) and $4_{0.49}\text{F}2_{0.51}$ (30 min soaking at $100\text{ }^\circ\text{C}$), are $5330\text{ m}^2\text{ g}^{-1}$ and $5500\text{ m}^2\text{ g}^{-1}$, respectively, which strongly indicate that the partial transmetalation influenced both the framework stability of the shell region and also the framework stability of the core region of the structures. To check whether the framework stability of the core region benefited from the protection by the external shell crystal or arose from its inherent property, a ground sample of $4_{0.49}\text{F}2_{0.51}$ with an exposed internal core was prepared and the framework stability was investigated using TGA, VT-PXRD, and N_2 sorption. The thermal stabilities of both ground $4_{0.49}\text{F}2_{0.51}$ and unground $4_{0.49}\text{F}2_{0.51}$ were similar to each other, and behaved like a hybrid structure of **2** and **4** that reflected the metal ion mole fraction in the framework (Supporting Information, Figure S17). However, to our surprise, there was no significant difference in the TGA behaviors of the unground and the ground samples. In addition, as shown in the VT-PXRD patterns (Supporting Information, Figure S18), the

thermal stability of $4_{0.49}\text{F}2_{0.51}$ framework structure was significantly improved comparing to that of as-synthesized **2** and was comparable to as-synthesized **4**. Furthermore, the N_2 sorption behavior of ground $4_{0.49}\text{F}2_{0.51}$ was similar to that of unground $4_{0.49}\text{F}2_{0.51}$, even though the majority of the internal core regions of $4_{0.49}\text{F}2_{0.51}$ were exposed in the ground sample (Supporting Information, Figure S19). These observations suggest that the partial and the selective transmetalations in the Co(II)/Cu(II)- and Co(II)/Ni(II)-core–shell heterostructures influence both the external shell region and the internal core region of the MOFs. The framework stability of the core region is not from any protection by the stable external shell structure but is an inherent property.¹⁶

The large enough aperture diameter of the framework pores of the ITHD frameworks ($\sim 9\text{ \AA}$) suggests that the accessibility of the replacing metal ion in the DMF solvent to the paddle-wheel SBU sites on the external surface of the MOF crystal is not the main cause of the kinetically controlled selective transmetalation to the core–shell heterostructure. The selectivity is from the different reactivities of the paddle-wheel SBUs, depending on the location of the SBU sites in the MOF crystal. It is natural that the SBU sites on an external surface are much more flexible than those in an internal core, and these different flexibilities of the SBU sites lead to different kinetic reactivities of the framework metal ions and the selectivity of the transmetalation.

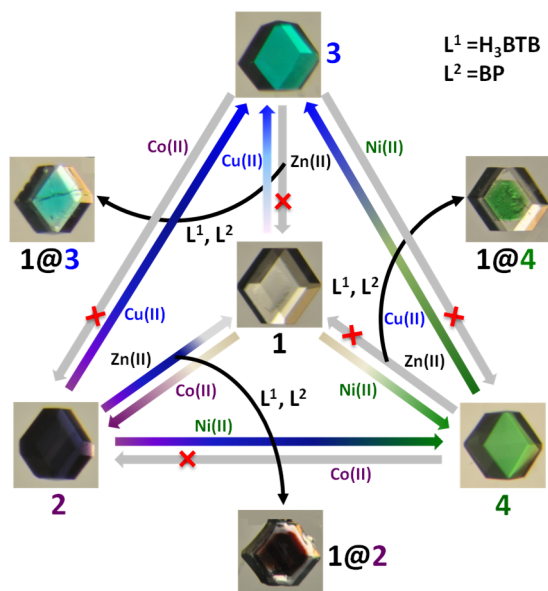
It is well-known that a core–shell heterostructure with a clear interface can be prepared via an epitaxial growth of a shell crystal on the surface of a core crystal.⁸ A series of core–shell heterostructures, **1@2**, **1@3**, and **1@4**, can be prepared using **2–4** as thermodynamically more stable core crystals, and **1** as a thermodynamically less stable shell crystal. Seeding **2–4** crystals as core crystals in a DMF solution of H_3BTB , BP, and $\text{Zn}(\text{NO}_3)_2 \cdot 6\text{H}_2\text{O}$ at an ambient temperature led **1** to grow epitaxially as a shell crystal on the surfaces of **2–4** seed crystals for 3 d. However, it is difficult to get the core–shell crystals as a pure phase in the epitaxial growth approach because the shell crystals are simultaneously obtained as a minor form. The distinctively different colors of the core and the shell crystals and the clear interfaces between the core and the shell crystals showed that **1** had grown epitaxially as a shell crystal on the surfaces of **2–4** (Supporting Information, Figure S20). However, while a core–shell heterostructure with a thermodynamically stable crystal as a core crystal and an equally stable, or less stable, crystal as a shell crystal can be prepared, it is not possible to generate the reverse core–shell heterostructure with a thermodynamically unstable crystal as a core crystal and a more stable crystal as a shell crystal. Seeding a thermodynamically unstable **1** in solutions of Co(II), Cu(II), and Ni(II) in the presence of H_3BTB and BP led to transmetalations rather than epitaxially grown core–shell heterostructures.

CONCLUSIONS

In a series of highly porous isostructural ITHD MOFs, framework metal ions of similar thermodynamic stabilities could be reversibly exchanged while keeping the integrity of the framework structures. Soaking the thermodynamically more stable ITHD crystals as a core crystal in metal ion solutions containing the framework metal ions of the potentially less stable ITHD crystals in the presence of ligands led to the epitaxially grown core–shell heterostructures. The reverse soaking, that is, soaking thermodynamically less stable ITHD crystals in metal ion solutions containing the framework metal

ions of the potentially more stable ITHD crystals in the absence of the ligands, led to the transmetalation of the framework metal ions while keeping the integrity of the framework structures (Scheme 1).

Scheme 1. Transmetalations and Epitaxial Growths of Core–Shell Crystals



By controlling the soaking time, either a homogeneous framework structure via complete transmetalation of the framework metal ion or a core–shell heterostructure via selective transmetalation mainly constrained to the external shell region of a crystal could be achieved. The selectivity of the transmetalation is not from the different accessibility of the replacing metal ion but from the different reactivities of the framework metal centers, depending on the location of the framework metal sites in the MOF crystal. This reflects the different flexibility of the framework metal sites. Framework metal sites with more flexible external surfaces reacted faster than framework metal sites in the more rigid internal core. This led to the different kinetic reactivities and the selectivity of the transmetalation.

The PXRD data of the as-synthesized MOFs with solvent in the pore showed the framework integrity in air at ambient temperature. However, when the solvent in the pore was gradually removed by applying heat during the VT-PXRD measurements, the water molecule present in air can react with the metal centers in the framework. The framework stabilities of the MOFs were not only governed by temperature but also affected by the reactivity of the metal centers with water. **4** showed excellent thermal stability; however, the other frameworks, **1–3**, had limited thermal stabilities in the presence of water because the metal centers in the frameworks were reactive to water to lose their structural integrities. However, the TGA result in N₂ environment showed different thermal stabilities of the framework structures. **3** showed increased thermal stability in absence of water; however, its thermal stability is still lower than that of **4** but higher than those of **1** and **2**. The VT-PXRD data in air and the TGA data in N₂ environment indicate that the order of the pure thermal stability of the MOFs is $4 > 3 \gg 2 \approx 1$. The N₂ uptake amounts and the BET surface areas of the isostructural MOFs

are closely related to the framework stabilities of the MOFs. The order of the framework stabilities based on the N₂ sorption behaviors of the MOFs, $4 > 3 \gg 2 > 1$, is also in good agreement with the observations from the TGA and the VT-PXRD.

In the cases of transmetalated $3_x\text{F}1_{1-x}$ and $4_x\text{F}1_{1-x}$ framework structures, the framework stability depends on the extent of the transmetalation of the framework metal ion at the external shell region of the crystal. The enhanced framework stability in the transmetalated shell region had the lowest influence on the stability of the less-affected internal core region. However, in the cases of the transmetalated core–shell heterostructures, $3_x\text{F}2_{1-x}$ and $4_x\text{F}2_{1-x}$, even partial transmetalation of the framework metal ions mainly in the external shell region of the crystal completely restored the framework stability of the as-synthesized framework structures. Not only the shell region but also the core region of the framework structure was influenced by the partial transmetalation.

Post-synthetic complete and/or selective transmetalations of the framework metal ions can be used as a general strategy for synthesizing highly porous MOFs with enhanced framework stabilities, and core–shell heterostructures with multifunctional properties.

■ ASSOCIATED CONTENT

📄 Supporting Information

A table of the BET specific surface area, Langmuir surface area, and the total pore volume of $3_x\text{F}1_{1-x}$ and $3_x\text{F}2_{1-x}$; TGA data of **1–4**, and ground and unground $4_{0.49}\text{F}2_{0.51}$; PXRD of **1F**₂₀ and **2F**₁₀, **3F**₁₀, **3F**₂₀, $3_{0.83}\text{F}4_{0.17}$, **4F**₁₀, **4F**₂₀; VT-PXRD of **1–4**; framework metal ion contents during the transmetalation for the framework structures from **1** to **3**, from **2** to **3**, from **1** to **4**, and from **2** to **4**; optical microscopic photographs of face-cut $3_{0.20}\text{F}1_{0.80}$, $3_{0.29}\text{F}1_{0.71}$, and $4_{0.34}\text{F}2_{0.66}$ crystals; optical microscopic photographs of core–shell crystals of **1@2**, **1@3**, and **1@4**; N₂ sorption isotherms of $3_{0.83}\text{F}4_{0.17}$. This material is available free of charge via the Internet at <http://pubs.acs.org>.

■ AUTHOR INFORMATION

✉ Corresponding Author

*E-mail: mslah@unist.ac.kr.

Notes

The authors declare no competing financial interest.

■ ACKNOWLEDGMENTS

This work was supported by NRF-2011-0027950 and WCU programs (R31-2011-000-20012-0) through the National Research Foundation of Korea.

■ ABBREVIATIONS

MOFs, metal–organic frameworks; SBU, secondary building unit; PSM, post-synthetic modification; CVD, conventional vacuum drying; SCD, supercritical carbon dioxide drying; BET, Brunauer–Emmett–Teller; TGA, thermal gravimetric analysis; PXRD, powder X-ray diffraction; VT-PXRD, variable temperature PXRD; ICP-AES, inductively coupled plasma atomic emission spectrometer; BTB, 1,3,5-benzenetribenzoate; BP, 4,4'-dipyridyl; DMF, *N,N'*-dimethylformamide; MC, dichloromethane

■ REFERENCES

- (1) Cohen, S. M. *Chem. Rev.* **2012**, *112*, 970–1000.

(2) (a) Wang, Z.; Cohen, S. M. *J. Am. Chem. Soc.* **2007**, *129*, 12368–12369. (b) Kiang, Y.-H.; Gardner, G. B. *J. Am. Chem. Soc.* **1999**, *121*, 8204–8215. (c) Seo, J. S.; Whang, D.; Lee, H.; Jun, S. I.; Oh, J.; Jeon, Y. J.; Kim, K. *Nature* **2000**, *404*, 982–986. (d) Haneda, T.; Kawano, M.; Kawamichi, T.; Fujita, M. *J. Am. Chem. Soc.* **2008**, *130*, 1578–1579. (e) Yamada, T.; Kitagawa, H. *J. Am. Chem. Soc.* **2009**, *131*, 6312–6313.

(3) (a) Shultz, A. M.; Sarjeant, A. A.; Farha, O. K.; Hupp, J. T.; Nguyen, S. T. *J. Am. Chem. Soc.* **2011**, *133*, 13252–13255. (b) Zhang, Z.; Zhang, L.; Wojtas, L.; Nugent, P.; Eddaoudi, M.; Zaworotko, M. J. *J. Am. Chem. Soc.* **2012**, *134*, 924–927.

(4) (a) Mulfort, K. L.; Farha, O. K.; Stern, C. L.; Sarjeant, A. A.; Hupp, J. T. *J. Am. Chem. Soc.* **2009**, *131*, 3866–3868. (b) Bloch, E. D.; Britt, D.; Lee, C.; Doonan, C. J.; Uribe-Romo, F. J.; Furukawa, H.; Long, J. R.; Yaghi, O. M. *J. Am. Chem. Soc.* **2010**, *132*, 14382–14384. (c) Oisaki, K.; Li, Q.; Furukawa, H.; Czaja, A. U.; Yaghi, O. M. *J. Am. Chem. Soc.* **2010**, *132*, 9262–9264.

(5) (a) Burnett, B. J.; Barron, P. M.; Hu, C.; Choe, W. *J. Am. Chem. Soc.* **2011**, *133*, 9984–9987. (b) Guillerm, V.; Gross, S.; Serre, C.; Devic, T.; Bauerc, M.; Férey, G. *Chem. Commun.* **2010**, *46*, 767–769. (c) Kim, M.; Cahill, J. F.; Su, Y.; Prather, K. A.; Cohen, S. M. *Chem. Sci.* **2012**, *3*, 126–130. (d) Burnett, B. J.; Choe, W. *Dalton Trans.* **2012**, *41*, 3889–3894.

(6) (a) Das, S.; Kim, H.; Kim, K. *J. Am. Chem. Soc.* **2009**, *131*, 3814–3815. (b) Mukherjee, G.; Biradha, K. *Chem. Commun.* **2012**, *48*, 4293–4295. (c) Huang, S.; Li, X.; Shi, X.; Hou, H.; Fan, Y. *J. Mater. Chem.* **2010**, *20*, 5695–5699. (d) Prasad, T. K.; Hong, D. H.; Suh, M. P. *Chem.—Eur. J.* **2010**, *16*, 14043–14050. (e) Dinca, M.; Long, J. R. *J. Am. Chem. Soc.* **2007**, *129*, 11172–11176. (f) Mi, L.; Hou, H.; Song, Z.; Han, H.; Xu, H.; Fan, Y.; Ng, S. W. *Cryst. Growth Des.* **2007**, *7*, 2553–2561. (g) Mi, L.; Hou, H.; Song, Z.; Han, H.; Fan, Y. *Chem.—Eur. J.* **2008**, *14*, 1814–1821.

(7) (a) Gadzikwa, T.; Lu, G.; Stern, C. L.; Wilson, S. R.; Hupp, J. T.; Nguyen, S. T. *Chem. Commun.* **2008**, *43*, 5493–5495. (b) Kondo, M.; Furukawa, S.; Hirai, K.; Kitagawa, S. *Angew. Chem., Int. Ed.* **2010**, *49*, 5327–5330. (c) Liu, B.; Ma, M.; Zacher, D.; Bétard, A.; Yussenko, K.; Metzler-Nolte, N.; Wöll, C.; Fischer, R. A. *J. Am. Chem. Soc.* **2011**, *133*, 1734–1737. (d) Zacher, D.; Schmid, R.; Wöll, C.; Fischer, R. A. *Angew. Chem., Int. Ed.* **2011**, *50*, 176–199. (e) Bétard, A.; Fischer, R. A. *Chem. Rev.* **2012**, *112*, 1055–1083.

(8) (a) Furukawa, S.; Hirai, K.; Nakagawa, K.; Takashima, Y.; Matsuda, R.; Tsuruoka, T.; Kondo, M.; Haruki, R.; Tanaka, D.; Sakamoto, K.; Shimomura, S.; Sakata, O.; Kitagawa, S. *Angew. Chem., Int. Ed.* **2009**, *48*, 1766–1770. (b) Hirai, K.; Furukawa, S.; Kondo, M.; Uehara, H.; Sakata, O.; Kitagawa, S. *Angew. Chem., Int. Ed.* **2011**, *50*, 8057–8061. (c) Koh, K.; Wong-Foy, A. G.; Matzger, A. J. *Chem. Commun.* **2009**, *41*, 6162–6164. (d) Yoo, Y.; Jeong, H. *Cryst. Growth Des.* **2010**, *10*, 1283–1288.

(9) Gadzikwa, T.; Farha, O. K.; Malliakas, C. D.; Kanatzidis, M. G.; Hupp, J. T.; Nguyen, S. T. *J. Am. Chem. Soc.* **2009**, *131*, 13613–13615.

(10) (a) Han, D.; Jiang, F.-L.; Wu, M.-Y.; Lian Chen, L.; Chen, Q.-H.; Hong, M.-C. *Chem. Commun.* **2011**, *47*, 9861–9863. (b) Klein, N.; Senkowska, I.; Baburin, I. A.; Grnker, R.; Stoeck, U.; Schlichtenmayer, M.; Streppel, B.; Mueller, U.; Leoni, S.; Hirscher, M.; Kaskel, S. *Chem.—Eur. J.* **2011**, *17*, 3007–3016.

(11) (a) Chen, B.; Eddaoudi, M.; Hyde, S. T.; O’Keeffe, M.; Yaghi, O. M. *Science* **2001**, *291*, 1021–1023. (b) Blatov, V. A. *IUCr CompComm Newsletter* **2006**, *7*, 4 ; TOPOS is available at <http://www.topos.ssu.samara.ru/>.

(12) Yao, Q.; Sun, J.; Li, K.; Su, J.; Peskova, M. V.; Zou, X. *Dalton Trans.* **2012**, *41*, 3953–3955.

(13) *Materials Studio program*, version 4.3; Accelrys: San Diego, CA, 2008.

(14) (a) Nelson, A. P.; Farha, O. K.; Mulfort, K. L.; Hupp, J. T. *J. Am. Chem. Soc.* **2009**, *131*, 458–460. (b) Farha, O. K.; Hupp, J. T. *Acc. Chem. Res.* **2010**, *43*, 1166–1175.

(15) The high framework stability of **3** activated via the SCD (at 40 °C) as shown by the N₂ sorption data (Figure 3 and Table 1), in addition to its TGA behavior, indicates that the limited thermal

stability of **3** in VT-PXRD is probably not from its inherent thermal property but from the instability of the framework in the presence of the water molecules in air during the VT-PXRD experiments.

(16) The core–shell heterostructures prepared via selective transmetalations do not have clear core–shell interfaces, unlike the core–shell heterostructures prepared via epitaxial growth. The optical microscopic photographs of the partially transmetalated $1_x\text{F}2_{1-x}$, $3_x\text{F}2_{1-x}$ and $4_x\text{F}2_{1-x}$ crystals (Figures 4b, 6b and 9b) and the face-cut $3_{0.34}\text{F}1_{0.66}$, $3_{0.34}\text{F}1_{0.66}$, and $4_{0.34}\text{F}1_{0.66}$ crystals (Supporting Information, Figures S21–23) show color gradients at the interfaces between the external surface and the internal core regions. The color gradients at the interfaces probably reflect the gradients in the mole fractions of the metal ions with the higher mole fraction of transmetalated metal ion occurring at the external shell region, and the lower mole fraction occurring in the internal core region. The framework stabilities of the Cu(II)/Co(II)- and the Ni(II)/Co(II)-core–shell heterostructures with lower mole fractions of Cu(II) and Ni(II) ions in the internal core regions are significantly enhanced. Even a minimum mole fraction of the transmetalated metal ion in the internal core region can have a significant effect on the framework stability of the internal core region of the core–shell heterostructure.